

Article

Sepiolite and Other Authigenic Mg-Clay Minerals Formation in Different Palustrine Environments (Madrid Basin, Spain)

Juan Emilio Herranz and Manuel Pozo * 

Department of Geology and Geochemistry, Faculty of Sciences, Autonomous University of Madrid, Campus de Cantoblanco, 28049 Madrid, Spain; juan.herranz@uam.es

* Correspondence: manuel.pozo@uam.es

Abstract: Lithofacies belonging to mud-flat and palustrine deposits (lake margin) in the Miocene of the Madrid Basin (Spain) have been studied. Four lithofacies corresponding to mud flat (1 and 3) and palustrine (2 and 4) deposits have been differentiated. Units 1 and 3 consist mainly of mudstones and carbonates (calcretes and diolocretes). The clay fraction is dominated by trioctahedral smectite (up to 79%) with illite and kaolinite as minor components. The d(060) spacing value shows reflections at 1.52 and 1.50 Å indicating also the presence of dioctahedral phyllosilicates. Unit 2 consists predominantly of lutites (claystones), locally with carbonate and chert nodules. The clay fraction is dominated by sepiolite (up to 96%) with variable contents of smectite and subordinate illite. The d(060) spacing value shows reflections at 1.51 and 1.52 Å indicating trioctahedral clay minerals. Unit 4 consists mostly of carbonates (limestones) with mudstone and lutite inserts. The clay fraction shows different contents of sepiolite, palygorskite and dioctahedral smectite. The analysis of a selection of trace elements (Cr, Co, Th, La, Sc) has allowed us to determine the characteristics of the source area as dioritic, somewhat different from those of the nearby materials from the Batallones sector. Sepiolite shows FWHM values ranging between 0.68 and 1.10 (2 θ), indicating “low crystallinity sepiolite”. Differences in the conditions of formation of magnesian smectite and palygorskite have been observed in the mud-flat and palustrine deposits. The formation of sepiolite mainly by neoformation in palustrine deposits with different hydrochemistry is remarkable, leading to differences in fibre size and crystallinity of the fibrous clay mineral. Authigenic transformation processes from previous Al-rich phases would be responsible for the formation of saponite and palygorskite in mud flat and palustrine environments, with different pH conditions.

Keywords: Miocene; palustrine environment; Mg-clays formation; sepiolite; palygorskite; smectite



Citation: Herranz, J.E.; Pozo, M. Sepiolite and Other Authigenic Mg-Clay Minerals Formation in Different Palustrine Environments (Madrid Basin, Spain). *Minerals* **2022**, *12*, 987. <https://doi.org/10.3390/min12080987>

Academic Editor: Jinwook Kim

Received: 3 July 2022

Accepted: 2 August 2022

Published: 3 August 2022

Publisher's Note: MDPI stays neutral with regard to jurisdictional claims in published maps and institutional affiliations.



Copyright: © 2022 by the authors. Licensee MDPI, Basel, Switzerland. This article is an open access article distributed under the terms and conditions of the Creative Commons Attribution (CC BY) license (<https://creativecommons.org/licenses/by/4.0/>).

1. Introduction

Clay authigenesis mostly concerns two main processes [1–3]: (a) formation of clays by direct precipitation from solution, called ‘neoformation’, and (b) development of clays by transformation of precursor, e.g., pyroclastics and detrital clays. Regarding the former process, direct precipitation from solution containing either simple or complex ions implies that a new mineral structure crystallizes, so that a pre-existing mineral structure is not inherited. Formation of minerals from solution is mainly controlled by kinetics. Once nucleation has taken place, crystal growth can be accomplished either by addition of ions and/or molecules to the surface of crystal nuclei (“classical” crystal growth; [4]) or via the aggregation and subsequent attachment of crystal nuclei together (‘nanoparticle’ behavior; [5]). Authigenic clays can form also by transformation of precursor, detrital minerals in both alkaline lakes and marine basins. This process was termed ‘neoformation by addition [1]’; the mechanisms involved are still a matter of discussion and several explanations have been proposed [6]. More recently, an update of the subject has been provided [7] pointing out the diffuse boundaries between the mechanisms of epitaxy (precipitation on pre-existing natural surfaces) and topotaxy (transformation and reaction

of pre-existing surfaces) as processes leading to formation of authigenic silicates after detrital clay precursors.

The Mg-clay minerals (sepiolite, palygorskite, Mg-smectite, kerolite) are an excellent example of authigenic clay minerals. Within magnesium clay minerals there are fibrous phases, such as sepiolite or palygorskite, and non-fibrous phases, such as magnesium smectites and kerolite [8]. The genetic relationship between fibrous and non-fibrous magnesium clay minerals has been discussed in several research papers ([9,10] and references therein), with the coexistence of different magnesium clay phases in the same deposit being relatively common. Three possible genetic mechanisms of sepiolite formation have been reported ([3] and references therein): direct precipitation from some fluid rich in Mg and Si (neof ormation), growth from gels formed by hydrated magnesium silicates and dissolution of precursor magnesium clay minerals with later sepiolite precipitation (transformation). The conditions necessary for the formation of sepiolite are based on the presence of a fluid with a moderate to high basic pH, adequate concentrations of magnesium and silica, and the absence of dissolved aluminium [3].

In this work, the formation of sepiolite and other magnesian clay minerals is studied in palustrine deposits characterized by different lithofacies associations. On the basis of mineralogical analyses, the aim is to establish if sepiolite formation is possible in similar sedimentological settings but with differences in the physical-chemical conditions of the sedimentary environment.

2. Geological Setting

The occurrence of large deposits of magnesian clays is one of the most remarkable features of the Neogene sediments in the Madrid Basin (Spain). The basin is located in the centre of the Iberian Peninsula and covers more than 10,000 km². It is one of the three main Cenozoic continental basins formed as a result of intense Cenozoic Alpine deformation within the Iberian microplate driven by the Africa–Eurasia collision [11].

The contrasting lithological composition of the basin margins strongly controlled the mineralogical and lithological features of the sedimentary deposits supplied to the basin [12] (Figure 1). Granites and high-grade metamorphic rocks formed the area of high relief to the W and NW, i.e., the Central System. Low-grade metamorphic rocks and sedimentary formations formed lower relief margins in the easternmost part of the Central System and the Iberian Range, respectively. Mesozoic sedimentary formations were exposed in the eastern part of the basin (Iberian and Altomira ranges). The Montes de Toledo to the south are composed mainly of granites and high-grade metamorphic rocks.

During most of the Neogene, the basin was occupied by lacustrine and palustrine systems fringed by alluvial fan and fluvial distributary facies forming a centripetal drainage system [13].

The Mg-clay deposits are located in a transition zone between alluvial and marginal lacustrine deposits mostly within the Miocene Intermediate Unit. These deposits occur in different lithofacies that are laterally equivalent, restricted to the northwest and especially south-southwest of the basin. The lithofacies association bearing Mg-clays was named “Magnesian Unit” by [14] in reference to its high Mg content. The Magnesian Unit facies are interpreted as alluvial-related, dry mudflat-to-palustrine deposits formed in a saline-alkaline lake margin. Within the Magnesian Unit, various non-fibrous Mg clays (saponite, stevensite, mixed layered kerolite/stevensite) have been recognized besides sepiolite [3,15], often forming economic deposits of bleaching earths (kerolite-stevensite clays) and Mg-bentonites (Figure 1).

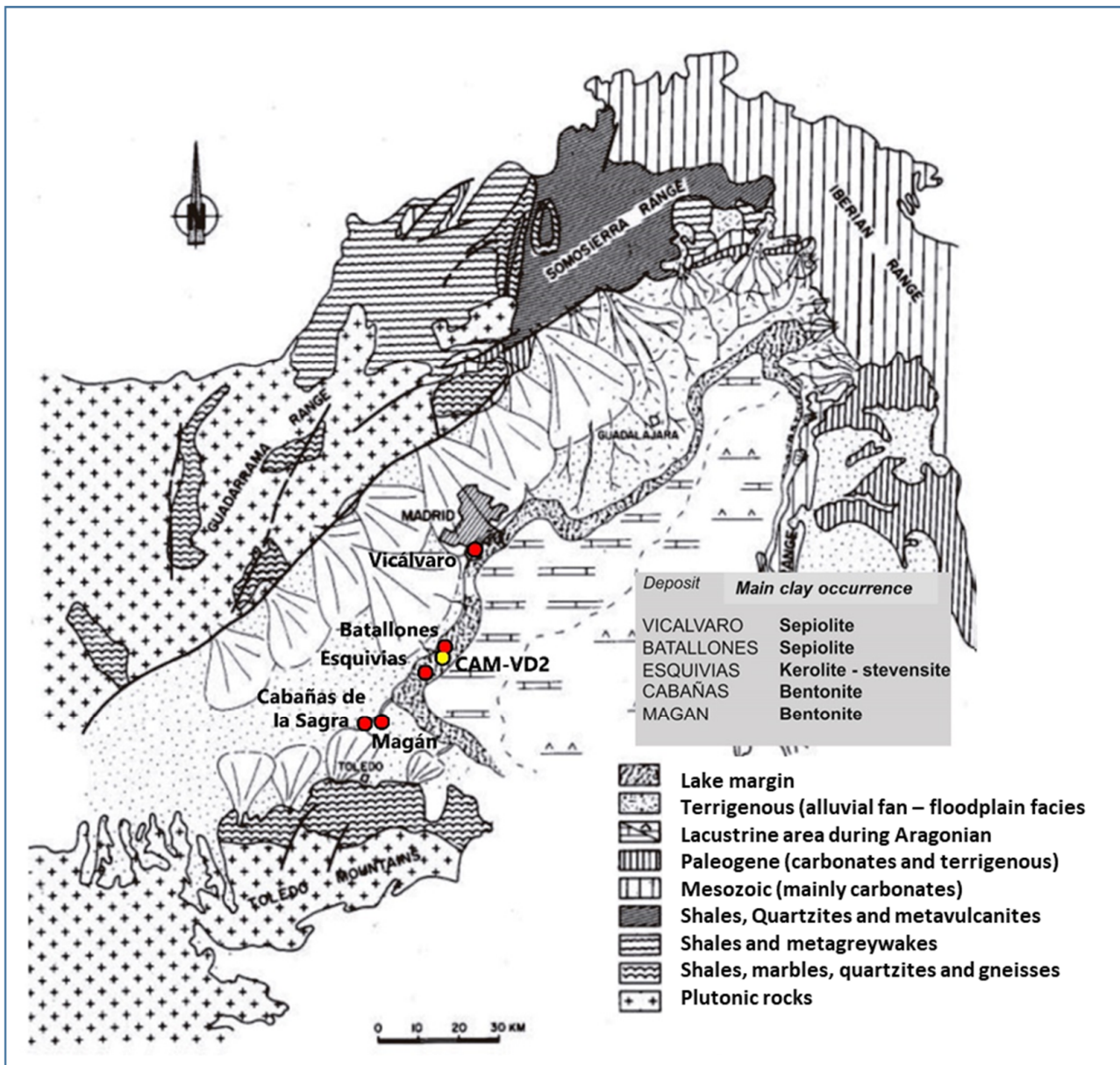


Figure 1. Paleogeographic reconstruction of the Madrid Basin during the Middle Miocene (modified from [16]). The position of the main deposits of magnesian clays (Magnesian Unit) is indicated, including the sector studied in this work (CAM-VD2).

3. Materials and Methods

3.1. Sampled Materials

The materials studied belong to the Miocene Intermediate Unit and their outcrops are located to the south of the Cerro de los Batallones sepiolite deposit [17] in an area called Campanillas-Valdedos (CAM-VD2) where the existence of quarry fronts has allowed a detailed sampling to be carried out (Figure 2A). The four different stratigraphic units have been established from two well-correlated lithological sections called CAM (Campanillas) and VD2 (Valdedos), a total of 42 samples being collected (Figure 3).

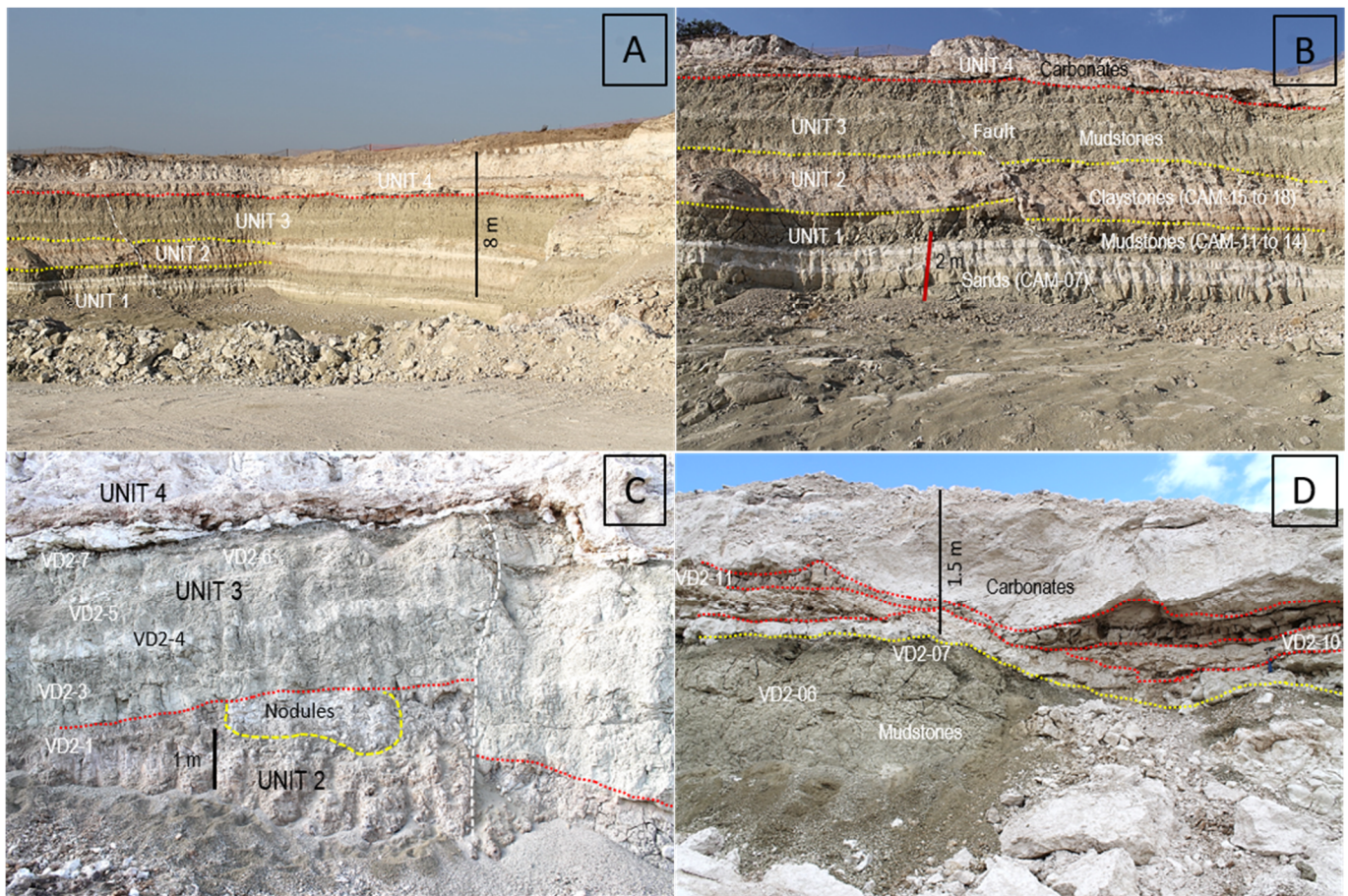


Figure 2. Field photographs showing the different units differentiated in the Valdedos-Campanillas lithostratigraphic section. (A) General view of the quarry front under study. (B) Lithofacies and contacts between units. The existence of a fault prior to unit 4 is observed. (C) Detail of the contact between units 2, 3 and 4. The presence of irregularly distributed nodules in unit 2 stands out. (D) Close-up of the contact between units 3 and 4. The lutite intercalations can be seen between the carbonates.

3.2. Experimental Methodology

Mineralogical analysis of 36 samples and 6 sub-samples was carried out by means of X-ray diffraction (XRD) using SIEMENS D-5000 equipment (Siemens AG, Gerätewerk-Karlsruhe, Germany) with a scanning speed of $1^\circ 2\theta/\text{min}$ and $\text{Cu-K}\alpha$ radiation (40 kV, 20 mA). The powdered whole-rock samples were used to determine bulk mineralogy. After clay fraction separation ($<2\ \mu\text{m}$), 23 sample mounts were prepared from suspensions oriented on glass slides. The identification of the clay minerals was carried out on oriented mounts of air-dried sample, with ethylene glycol solvation, and heated at $550\ ^\circ\text{C}$. The mineral-intensity factors (MIF) method was applied to XRD reflection-intensity ratios normalized to 100% with calibration constants for the quantitative estimation of mineral contents ([18–20]). To establish the relative ordering and/or crystal size (“crystallinity”) of sepiolite, the FWHM (Full Width at Half Maximum) parameter was measured on the (110) reflection at $12\ \text{Å}$ in the bulk sample [21]. Variation in “crystallinity” is a common feature in sepiolite that has been observed in many deposits world-wide [3].

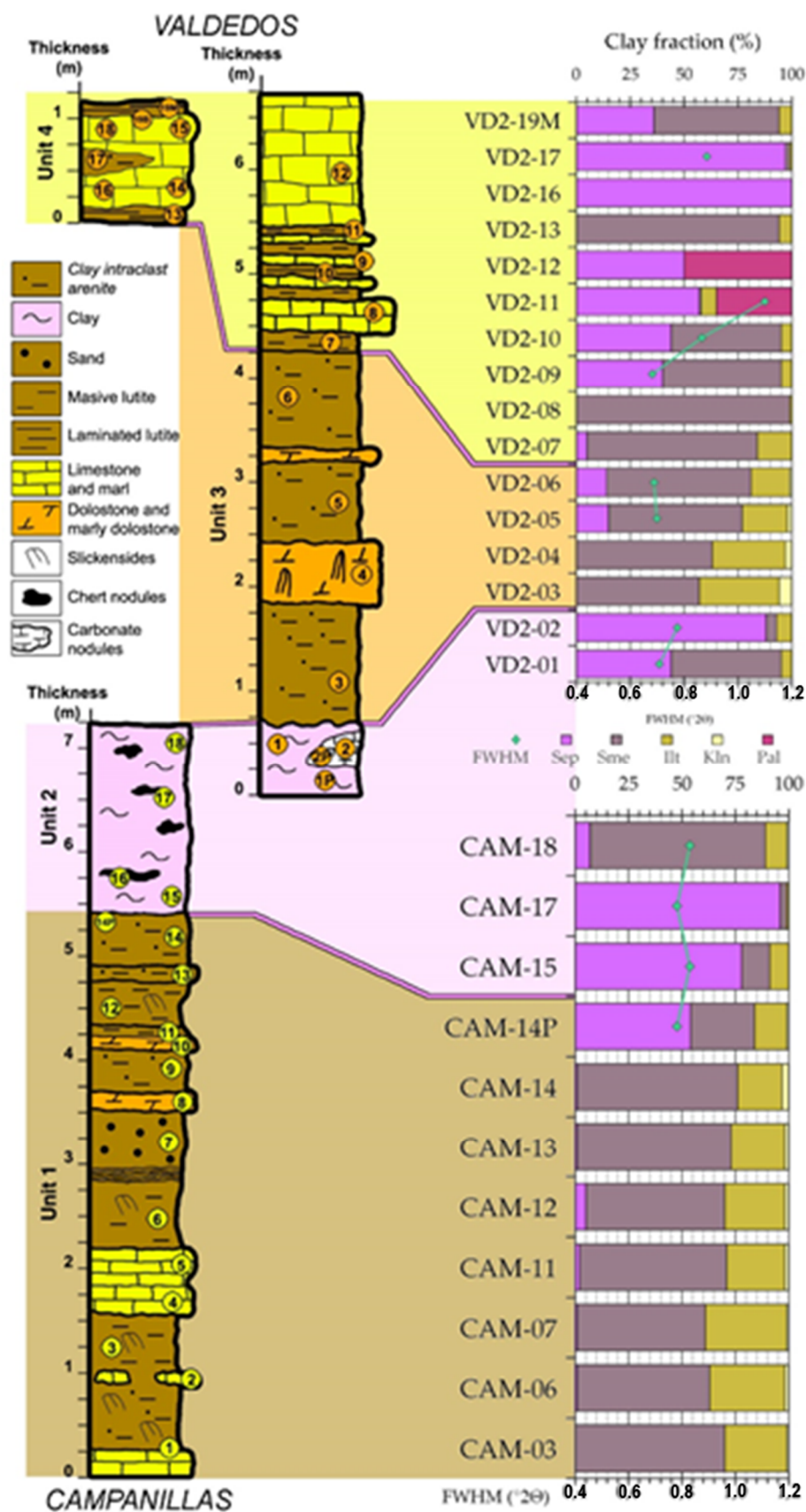


Figure 3. Lithostratigraphic log and clay fraction mineralogy of the VD2 and CAM sections. The correlation of the different units, samples position and sepiolite FWHM values are also indicated.

The chemical analysis of major elements and selected trace elements (Cr, Th, Sc, Co and La) of 16 samples from VD2-CAM section was performed by means of the MagiX X-ray fluorescence (XRF) spectrometer (PANalytical, Almedo, The Netherlands) of PANalytical. The determination of major elements was carried out by fusion with lithium tetraborate at a ratio of 0.3:0.55 (sample:flux). Trace elements were determined in pressed tablets with elvacite. The loss on ignition was carried out gravimetrically by calcination at 950 °C. A Varian 220-FS QU-106, atomic absorption (AA) spectrophotometer (Varian, Inc., Victoria, Australia) was used for the determination of sodium.

Seven selected samples were examined under SEM (Philips SEM XL-30, Philips, Eindhoven, The Netherlands) after coating with gold (10 nm thick) in a sputtering chamber.

4. Results and Discussion

4.1. Description of Lithofacies in the Differentiated Units

Unit 1 is about 5 m thick and consists of several sequences starting with greenish to brownish mudstones (<1 m thick) and ending with marly levels (<0.5 m thick), of calcite and dolomite composition (Figure 2B). The following lithofacies have been differentiated: marly limestone (CaMa), marly dolomite (MaDo), sandy dolomitic marl (SdDoMa), sandstone (Sd), clay intraclast arenite (Md(i)), massive mudstone (Md) and laminated mudstone (Md(l)). In this unit, 15 samples were collected, all in the CAM section.

Unit 2 is made up of about 2 m of pinkish lutites (clays or claystones) (Md, Md(l)) locally presenting centimetric chert nodules and limited to the top by an erosive surface. Laterally, nodules of decimetric dolomite carbonates are included in the clayey material, and more occasionally smaller calcite nodules can also be observed. The main lithofacies are lutites (Md, Md(l)) accompanied by chert and carbonate nodules (Figure 2B,C). In this unit, 8 samples have been taken, distributed between the two sections sampled (CAM and VD2).

Unit 3 is composed of almost 4 m of yellowish-green mudstones and white carbonate levels (0.2–0.6 m thick), forming sequences (Figure 2B,C). The following lithofacies have been differentiated: mudstones (Md), clay intraclast arenites (Md(i)) and marly dolomites (MaDo). In this unit, 5 samples have been taken, all of them in section VD2.

Unit 4 is almost 4 m thick and mainly consists of bedded to massive calcareous carbonates (0.3 to 3 m thick) with lenticular inserts of massive to laminated lutites (claystones) (<0.20 thick). In these carbonates there are abundant traces of root bioturbation and evidence of reworking (Figure 2D). Laterally, non-stratified carbonate accumulations have been observed. Several lithofacies have been differentiated: limestones (Lm), massive lutites (Md) and laminated lutites (Md(l)). In this unit, 13 samples have been collected, all of them in section VD2.

4.2. Mineralogical Assemblages and Sedimentary Environment

The mineralogical composition and content of major chemical elements are given in Tables 1 and 2, respectively.

4.2.1. Unit 1

Unit 1 is formed by sequences in which massive to laminated mudstones or clastic lithofacies (sandstones or clay clast arenites) originate sequences with carbonated marly lithofacies (Figure 3). The massive and granular mudstones (clay intraclast arenites) have a high phyllosilicate content (85%–100%) with low quartz and feldspar content (Id-7%) and locally calcite (13%). The carbonate levels show calcite percentages reaching 44% where the existence of zones richer in phyllosilicates, especially at the base of the beds, evidences that the identified calcite is the result of a process of carbonation under paleosol conditions (calcretes).

In the sand beds, the high content of quartz (up to 17%) and feldspars (up to 35%) stands out. Associated with the sandy deposits, there are dolomite-rich beds (up to 55%) with field features suggesting that dolocrete has been formed.

Table 1. Bulk mineralogy: phyllosilicates (Phy), quartz (Qz), feldspars (Fsp), calcite (Cal), dolomite (Dol). Clay mineralogy: smectite (Sme), sepiolite (Sep), illite (Ill), palygorskite (Pal), kaolinite (Kln). Lithologies: massive mudstone/lutite (Md), clay intraclast arenite (Md(i)), laminated mudstone/lutite (Md(l)), calcareous marl (CaMa), sandstone (Sd), sandy dolomitic marl (SdDoMa), marly dolostone (MaDo), marly limestone (MaLm), Limestone (Lm). Tr. Traces.

Unit	Sample	Lithology	Bulk Mineralogy (%)					Clay Fraction (%)				Sepiolite	
			Phy	Qz	Fsp	Cal	Dol	Sme	Sep	Ill	Pal	Kln	FWHM (°2 θ)
4	VD2-19M	Md	81	4	10	5		57	35	6			
4	VD2-19B	Lm	Tr			100							
4	VD2-18	Lm	Tr			100							
4	VD2-17	Md	92	4	4	Tr		2	98	Tr			0.884
4	VD2-16	Lm	11			89			100				
4	VD2-15	Lm	Tr			100							
4	VD2-14	Lm	8			92							
4	VD2-13	Md(l)	86	8	6			94		6			
4	VD2-12	Lm	25	5		70			50	Tr	50		
4	VD2-11	Md	92	4	4			1	57	7	35		1.100
4	VD2-10	Md(l)	89	4	5	2	Tr	51	44	5			0.866
4	VD2-09	MaLm	34			66		55	40	5			0.683
4	VD2-08	Lm	20	2		77	Tr	100		Tr			
3	VD2-07	Md	93	4	3			79	5	16			
3	VD2-06	Md(i)	90	4	6			67	14	18		1	
3	VD2-05	Md(i)	92	3	5			63	15	21		2	
3	VD2-04	MaDo	56	3	4		37	63		34		3	
3	VD2-03	Md	94	5	Tr		Tr	57		37		6	
2	VD2-02	Md	46	3			51	5	88	7			0.775
2	VD2-01	Md	89	6	5			52	44	5			0.708
2	VD2-01P	Nodule	27			73	Tr	57	35	6			
2	CAM-18	Md	100	Tr	Tr			82	7	10		Tr	0.830
2	CAM-17	Md	95	Tr	4		1	3	96	1			0.781
2	CAM-16	Md	100	Tr	Tr								
2	CAM-15	Md(l)	100	Tr	Tr			13	78	9		Tr	0.830
2	CAM-15C	Md	100	Tr	Tr			2	96	2			0.749
2	CAM-15B	Md	100	Tr	Tr			23	65	12		Tr	1.042
1	CAM-14P	Md(l)	100	Tr	Tr			31	54	15		Tr	0.782
1	CAM-14Pa	Md	100	Tr	Tr			20	72	8			0.739
1	CAM-14Pb	Md	100	Tr	Tr			37	46	16		1	0.782
1	CAM-14Pc	Md	100	Tr	Tr			74	4	21		1	
1	CAM-14	Md(i)	100	Tr	Tr			75	Tr	22		3	
1	CAM-13	Md(i)	96	Tr	Tr	4		72	1	25		2	
1	CAM-12	Md	100	Tr	Tr			65	5	28		2	
1	CAM-11	Md	100	Tr	Tr			69	2	27		2	
1	CAM-10	MaDo	45				55						
1	CAM-10B	Md	81	Tr	Tr		19						
1	CAM-09	SdDoMa	58	15	4		23						
1	CAM-08	SdDoMa	22	3	27		48						
1	CAM-07	Sd	48	17	35			60	Tr	39		1	
1	CAM-06	Md	93	4	3			62	Tr	36		2	
1	CAM-05	CaMa	69	2	1	28							
1	CAM-04	CaMa	56			44							
1	CAM-04B	Md	75	Tr		25							
1	CAM-03	Md	94	6	Tr			70		29		1	
1	CAM-02	Ma	56			44							
1	CAM-01	Md(i)	85	Tr	2		13						

Table 2. Chemical analysis (major elements % *w/w*).

Unit	Sample	Lithology	SiO ₂	MgO	Al ₂ O ₃	Fe ₂ O ₃	CaO	TiO ₂	K ₂ O	MnO	P ₂ O ₅	Na ₂ O	LOI
4	VD2-19	Md	35.71	9.22	6.04	2.04	17.44	0.27	0.62	<0.05	0.17	0.18	26.82
4	VD2-17	Md(i)	52.81	18.41	4.01	1.28	0.31	0.17	0.44	<0.05	0.05	0.16	20.85
4	VD2-13	Md(l)	48.46	13.68	7.70	2.25	0.65	0.35	0.82	0.05	0.05	0.26	25.33
4	VD2-11	Md	53.83	14.76	6.95	2.07	0.54	0.29	0.76	<0.05	0.24	0.18	18.89
4	VD2-10	Md(l)	50.90	10.44	9.73	3.29	1.74	0.43	1.07	<0.05	0.23	0.28	20.28
3	VD2-07	Md	51.18	9.76	11.95	4.02	0.78	0.46	1.91	<0.05	0.04	0.31	18.76
3	VD2-05	Md(i)	38.30	12.08	10.13	3.63	8.01	0.43	1.92	0.05	0.08	0.42	24.06
2	VD2-01	Md	51.68	18.58	5.60	1.93	0.41	0.25	0.68	<0.05	0.04	0.18	19.14
2	CAM-18	Md	47.60	13.00	8.98	3.07	0.45	0.37	1.08	<0.05	<0.05	0.16	25.50
2	CAM-17	Md	52.30	22.80	1.33	0.47	0.89	0.05	0.17	<0.05	<0.05	0.05	21.90
2	CAM-15	Md(l)	51.70	16.20	6.31	2.35	0.25	0.24	1.00	<0.05	<0.05	0.14	21.60
1	CAM-14P	Md(l)	48.10	12.60	8.05	2.96	0.28	0.30	1.25	<0.05	<0.05	0.14	25.60
1	CAM-14	Md(i)	47.90	11.70	10.30	3.83	1.07	0.36	1.50	<0.05	0.18	0.15	23.10
1	CAM-12	Md	44.80	10.30	10.40	3.76	0.68	0.32	1.61	<0.05	0.23	0.19	27.20
1	CAM-06	Md	47.50	8.80	13.90	5.34	0.44	0.49	2.76	<0.05	0.07	0.31	19.10
1	CAM-03	Md	48.30	10.30	13.40	5.19	0.62	0.54	2.49	0.05	0.14	0.35	18.70

The clay minerals identified in unit 1 present a simple mineral assemblage: smectite-illite-(kaolinite) (Table 1 and Figure 3). Smectite is the main mineral (31%–75%), always accompanied by illite (15%–39%) and traces of kaolinite (<5%) and possible sepiolite (<5%). With regard to the type of phyllosilicates, no special predominance of di- or trioctahedral phases is observed in the samples. Two reflections are observed at 1.525 Å and 1.501 Å of which the dioctahedral term would partly correspond to illite-mica. The existence of a trioctahedral component in the samples rich in smectite indicates processes of authigenic formation of magnesium smectite (saponite).

On top of the unit, the presence of a laminated bed (CAM-14P) showing the high textural heterogeneity and transitional characteristics of the materials of unit 2 has been observed laterally. Three zones of the same sample have been analyzed in order to determine the existence of variations in the mineralogical composition. The white laminar zones (CAM-14Pa) present a clay fraction association in which sepiolite predominates (72%), with lower contents of smectite (20%) and illite (8%). The greenish brecciated morphologies (CAM-14Pc) present a mineral association in which smectite (74%) and illite (21%) predominate with minor sepiolite and kaolinite (<5%). The areas of waxy lutite seem to have an intermediate composition (CAM-14Pb) with closer proportions of sepiolite (46%) and smectite (37%) with minor illite (16%) and traces of kaolinite. This mineralogical result points to an increase in the participation of authigenic processes, with the possible formation of sepiolite from Mg-smectite by transformation (dissolution-precipitation).

The representative XRD patterns of the two main clay mineral assemblages identified are shown in Figure 4. Observed with the SEM, the CAM-14P sample shows a laminar microfabric where lamellar morphologies of smectite and fibrous aggregates of sepiolite can be recognized (Figure 5A). In detail, sepiolite occurs in dense aggregates of small fibres (around 2 µm) (Figure 5B).

Taking into account the chemical analysis of major elements SiO₂ (44.80%–48.30%), MgO (8.80%–12.60%) and Al₂O₃ (8.50%–13.90%) are predominant (Table 2 and Figure 6). In percentages close to 5% or less, the remaining major elements (Fe₂O₃, CaO, TiO₂, K₂O, MnO, P₂O₅, Na₂O) are present. The vertical trend of contents shows an increase in MgO and a decrease in Al₂O₃ and the other major elements. These variations give rise to sequences due to dolomite formation and magnesian smectite formation in the deposits of the lacustrine margin.

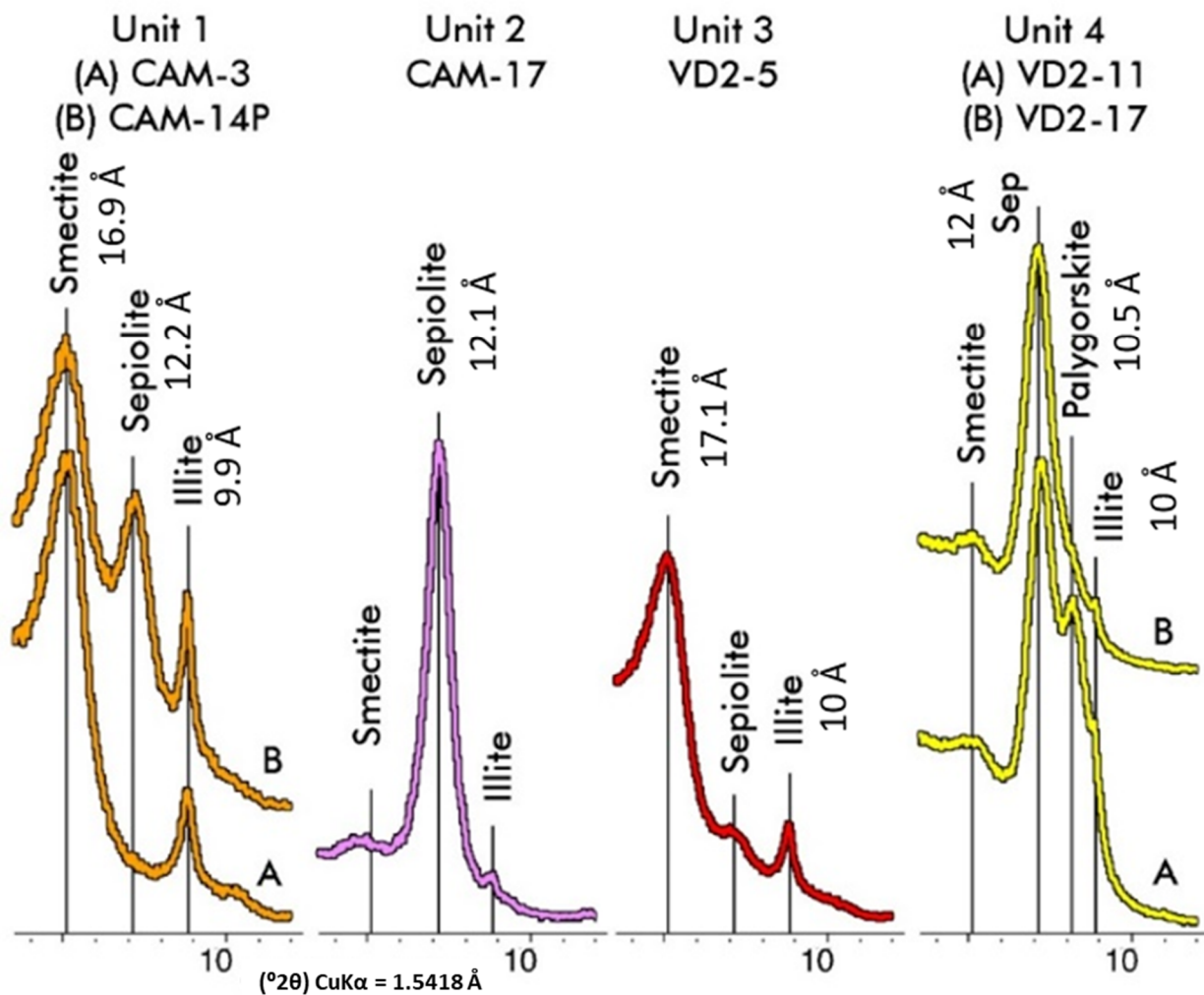


Figure 4. Representative XRD patterns (ethylene glycol oriented mounts) of the clay mineral assemblages in the differentiated units. The letters A and B indicate representative samples from the same unit. The sample plotted on the graph is indicated.

From a sedimentological point of view, the distribution of facies and their composition is interpreted as a mudflat environment with episodes of lake flooding followed by others of subaerial exposure, in which the precipitation of carbonates is favoured, affecting the lithofacies, originating calcretes and dolocretes. Locally, the occurrence of sandy deposits indicates the existence of detrital inputs that introduce inherited minerals into the sedimentary environment. At the top of the unit, the presence of sepiolite in conspicuous contents indicates authigenesis and a significant change in the physical-chemical conditions since its formation requires an adequate salinity, Mg/Si ratio, pH and availability of silica [3].

4.2.2. Unit 2

This unit is made up of pinkish lutites (clays or claystones) that occasionally include chert nodules, especially at the base of the section, and carbonate nodules at the top of the unit (Figure 3). The lutites show massive, laminated and brecciated lithofacies, with frequent clay intraclasts and evidence of bioturbation. Lutites are predominantly formed by phyllosilicates (>85%) with a very low content of quartz and feldspars (mainly plagioclase) that only reach contents close to 5% in contact with unit 3 (Table 1). Locally, pockets with carbonate nodules have been observed, in which dolomite (51%) is the principal mineral, accompanied by phyllosilicates (46%) and quartz (3%). At the top of the unit, coatings

have also been identified around silicified nodules (sample VD2-1P), with high contents of calcite (73%), accompanied by phyllosilicates (27%) and traces of dolomite.

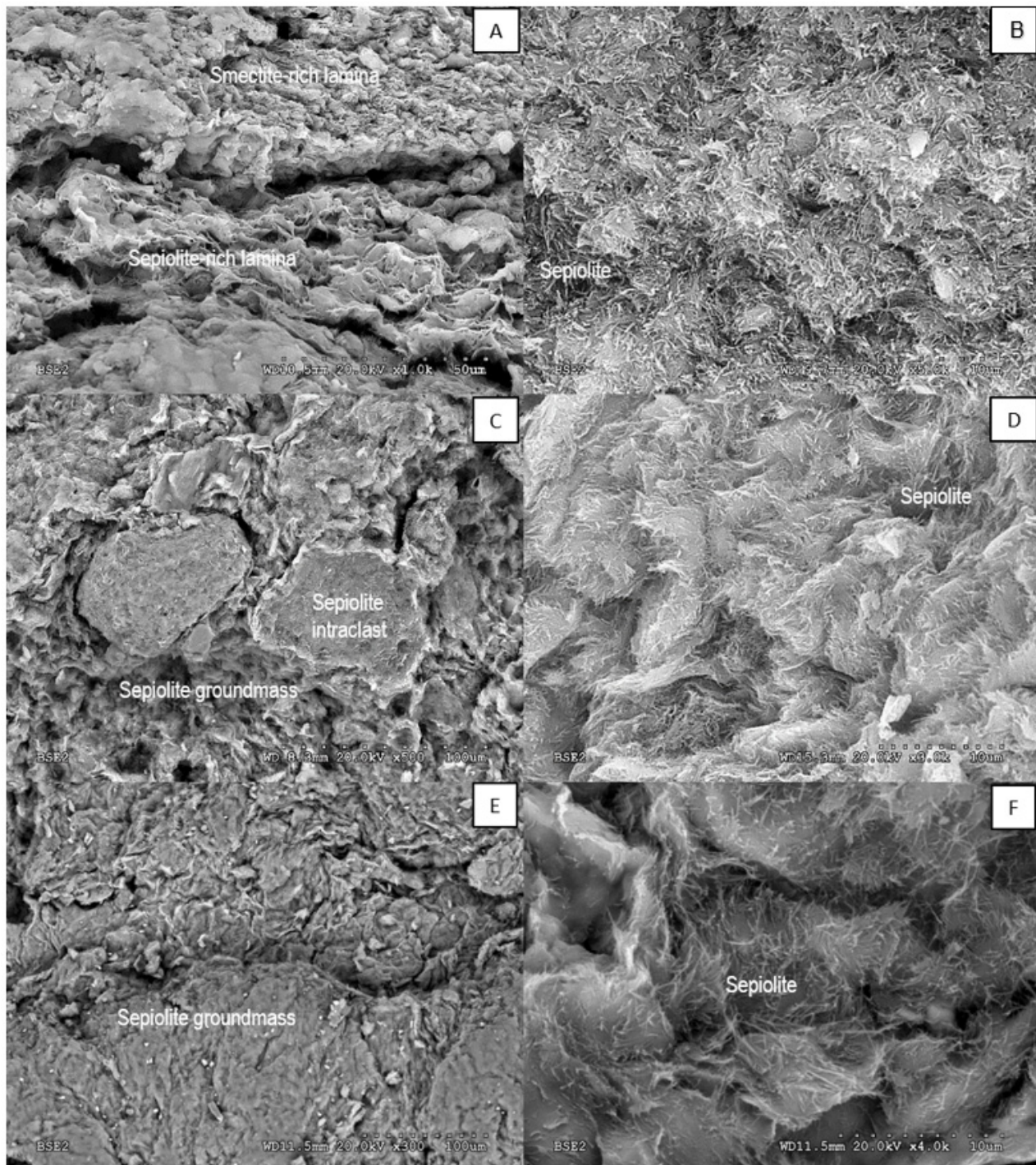


Figure 5. SEM images of representative samples with sepiolite. (A) Laminar microfabric showing differences in laminae composition suggesting a genetic relationship between smectite and sepiolite (CAM-14P). (B) Close-up of sepiolite showing dense short fibre (2 μm) bundles. (C) Matrix-skeletal microfabric showing sepiolite intraclasts within a sepiolite groundmass (VD2-1). (D) Close-up of dense larger fibre (5 μm) bundles. (E) Matrix-laminar microfacies in sepiolite-palygorskite groundmass (VD2-11). (F) Detail of bundles formed of relatively large (>5 μm) sepiolite fibres.

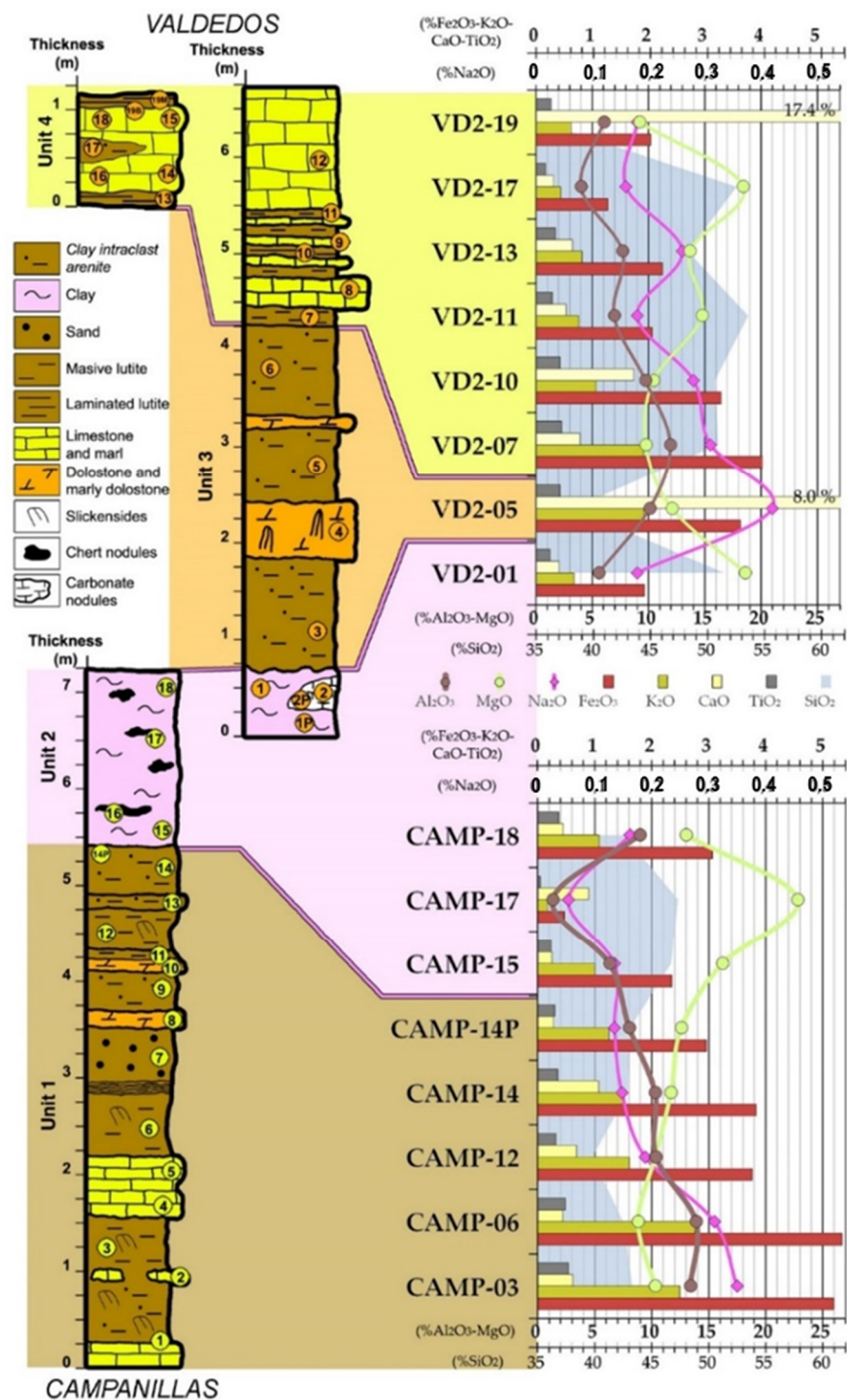


Figure 6. Graph showing the trend of major elements (% w/w).

In the clay fraction the mineral assemblage is: sepiolite-(smectite, illite) (Table 1 and Figure 3). Sepiolite is the main mineral (78%–96%), with smectite (2%–13%) and illite (1%–9%) as minor minerals. Locally, a second assemblage is only observed at the top of the unit (samples CAM-18 and VD2-1), where smectite becomes the main mineral (52%–82%), accompanied by minor sepiolite (7%–44%) and illite (5%–10%), with traces of kaolinite. This second assemblage seems to be related with contamination (mixture) from sediments of unit 3. The FWHM value for sepiolite (Table 1) ranges between 0.708 and 1.042 ($^{\circ}2\theta$), values that correspond to low “crystallinity” sepiolite (LCS), taking as a reference the reported values for sepiolites ([17,22]. The phyllosilicates show a predominance

of trioctahedral phyllosilicates with $d(060)$ ranging between 1.517 Å (sepiolite-rich) and 1.526 Å (smectite)-rich.

The basal sample of the unit (CAM-15) is laminated, and two materials of different appearance are observed. One is a greenish lutite (claystone), in layers of 2–3 cm thick (CAM-15B), and the other is a discontinuous intercalation of lesser thickness (2–4 mm) of white to pinkish lutite that may include intraclasts of the previous one (CAM-15C). The mineralogical study of 15B and C separately indicates that in both cases sepiolite is the predominant mineral (65%–96%), but sub-sample CAM-15B also presents kaolinite and contents of smectite (23%) and illite (12%) much higher than those of sub-sample CAM-15C (<5%). This sample has a transitional character equivalent to the CAM-14P sample, representing the passage from a mudflat environment to a palustrine one.

The representative XRD pattern of the main clay mineral assemblage identified is shown in Figure 4. Under SEM examination a matrix-skeletal microfabric is observed where sepiolite is identified in both clay intraclasts and groundmass, suggesting several stages of formation (Figure 5C). In detail, the sepiolite occurs in dense aggregates of fibres of moderate sizes (around 5 µm) (Figure 5D).

The contents of major elements in the samples of unit 2 show significant differences from unit 1 (Table 2 and Figure 6). Higher MgO contents (13.00%–22.80%) and lower Al₂O₃ contents (1.33%–8.98%) are observed. On the top, locally increased Al₂O₃ is observed as a result of contamination from the deposits of unit 3. The low Al₂O₃ content in some of the samples with magnesian smectite suggests the presence of stevensite rather than saponite.

The lithofacies occurring in unit 2 are interpreted as formed in a palustrine environment. The supply of silica and the development of nodular morphologies of dolomite and calcite composition would be indicative of groundwater input, possibly paleosprings forming seepage-mounds, which would favour the formation of Mg-clays, as those described in adjacent areas [23]. Excess silica in the absence of magnesium would justify the incipient nodular silicification of sepiolite.

4.2.3. Unit 3

Unit 3 has two lithofacies, forming sequences; one consisting of mudstones and the other of carbonates (Figure 3). The mudstone beds present common grain-supported intraclasts (clay intraclast arenites), with a silt- to clay-sized matrix. The carbonates are actually marly dolomites with clay clasts inclusions, suggesting dolocretes.

Phyllosilicates are the most abundant minerals (56%–94%), with low contents of quartz (3%–5%) and feldspars (≤6%, mainly plagioclase), whereas in carbonate levels the dolomite content is 37%. In the clay fraction only one mineralogical assemblage has been observed: smectite-illite-(kaolinite, sepiolite) (Table 1 and Figure 3). Smectite is the main clay mineral (57%–79%) with minor illite (21%–37%), sepiolite (up to 15%) and traces of kaolinite (<3%). Both di (1.503 Å) and trioctahedral (1.528 Å) phyllosilicates have also been identified. The representative XRD patterns of the clay-mineral assemblage identified is shown in Figure 4.

The chemical analysis of a representative sample of the lithofacies (VD2–5) shows similar contents of major elements to those observed in unit 1 (Al₂O₃ = 10.13% and MgO = 12.08%), although presenting a slightly lower SiO₂ content (38.3%) (Table 2 and Figure 6). Again, the formation of dolomite and magnesian smectite would account for the variations in the MgO/Al₂O₃ ratio.

As in the case of unit 1, the lithofacies deposited in a mudflat environment in which the carbonate levels would represent the moments of greatest exposure and evaporation that would favour the formation of dolocretes.

4.2.4. Unit 4

This unit consists predominantly of limestones with subordinate lutite inserts, especially at the base of the unit (Figure 3). The limestones form beds, although laterally, accumulations of carbonate can be observed which could correspond to paleo-spring morphologies (seepage mounds), as had been previously mentioned in nearby points [22]. From

the mineralogical point of view, the carbonates are predominantly formed by calcite both in the beds and in the mounds of carbonate accumulation (66%–100%). The phyllosilicate content is less than 35% and the quartz content does not exceed 5%, with traces of dolomite detected in some samples.

The lutites (claystones) have a phyllosilicate content ranging from 86 to 93%, with minor quartz (4%–8%), feldspars (4%–10%) and occasional traces of calcite and dolomite (<5%). In the bedded lutite inserts two clay mineralogical assemblages are differentiated (Table 1, Figure 3): 1-smectite-sepiolite-(illite); 2-sepiolite-palygorskite-(illite). In the lower assemblage (VD2-7, 9,10), smectite (51%–79%) predominates with sepiolite (5%–44%) and illite (5%–16%) in lower content. The upper assemblage (VD2-11, 12) consists of sepiolite (50%–57%) and palygorskite (35%–50%) with a low content of illite (<10%) and traces of smectite.

A third clay mineral assemblage is identified associated to carbonate mounds (VD2-14 to 19): sepiolite-(smectite-illite). The main clay mineral is sepiolite with minor smectite (3%–58%) and illite (<10%). The existence of a fourth mineralogical assemblage (smectite-(illite)) stands out at the base of carbonate accumulation.

Due to the variety of established mineralogical associations no clear geochemical trends are observed, although CaO plays an important role. Chemical element contents are controlled by the type of authigenic mineral formed. The detrital influence is evident in the K₂O and Fe₂O₃ contents, also in the Al₂O₃ content in the more smectitic samples.

The representative XRD patterns of the two main clay mineral assemblages identified are shown in Figure 4. Under SEM examination a matrix to laminated microfabric is observed (Figure 5E). In detail, sepiolite occurs in dense aggregates of fibres with sizes commonly larger than 5 µm (Figure 5F). In the smectite-rich samples the d(060) value is 1.506 Å indicating that they are dioctahedral, with no trioctahedral smectites of the saponite type being formed.

The measurement of the FWHM value in 6 samples with sepiolite (Table 1) ranges from 0.683 to 1.100 (°2θ) which together with the poor development of its reflections indicates LCS-type sepiolite [17].

Unit 4 is related to a palustrine environment with relatively fresh waters in which the hydrochemical conditions would have been favourable for the formation of calcium carbonate. The involvement of groundwater input linked to paleo-springs could have played an important role.

4.3. Trace Elements and Source of Provenance

Trace element content can be a potential source of information on the origin of a certain type of sediment or rock [24]. Elements such as La, Th, Sc and, to a lesser extent, Cr and Co are also very useful trace elements. This is because they have a low solubility and, therefore, are not susceptible to leaching processes; their transport is associated with the movement of terrigenous materials, which enables the characteristics of their source area to be approximated [25,26]. The comparison of the contents of some trace elements present in acidic and basic rocks shows that La and Th are more abundant in the former, whereas Sc and Co are more abundant in the latter. This makes it possible to use elements such as Th and Sc, or ratios such as La/Sc and La/Co, to determine the type of source area with which a material is associated [27], so that a relative enrichment of compatible elements would indicate a felsic character of the source area.

Table 3 shows the chemical analyses of Cr, Th, Sc, Co and La. Based on the aforementioned trace elements, graphs have been made comparing the values of these samples with those already published in the nearby area of Cerro de los Batallones [22], in order to establish possible characteristics of the provenance area. As reference values, those published for several lithologies (granites and diorites) and the average values of the upper crust (UCC) [28] have been included.

Table 3. Selected trace elements for provenance interpretation. The values in parentheses correspond to the detection limits of the elements analysed with the technique used.

Unit	Sample	Lithology	Co (2.41)	Cr (1.50)	La (5.08)	Th (1.5)	Sc (2.47)
4	VD2-19	Md	<2.4	17.4	30.2	6.5	10.1
4	VD2-17	Md	2.9	4.5	9.0	4.2	<2.4
4	VD2-13	Md(l)	4.8	16.1	17.4	9.8	7.3
4	VD2-11	Md	<2.4	22.7	15.4	7.0	<2.4
4	VD2-10	Md(l)	4.4	31.7	24.1	12.4	8.2
3	VD2-07	Md	3.5	29.4	30.3	13.7	11.3
3	VD2-05	Md(i)	7.2	10.7	26.4	11.1	13.0
2	VD2-01	Md	<2.4	14.8	10.9	4.7	5.1
2	CAM-18	Md	4.8	26.2	15.0	7.2	9.6
2	CAM-17	Md	<2.4	1.8	3.0	<1.5	2.1
2	CAM-15	Md(l)	2.9	26.7	10.3	4.2	5.2
1	CAM-14P	Md(l)	3.5	42.5	13.1	6.3	7.2
1	CAM-14	Md(i)	7.3	18.0	25.8	8.5	9.3
1	CAM-12	Md	7.4	26.4	20.3	10.5	9.2
1	CAM-06	Md	8.9	34.8	24.9	11.2	12.3
1	CAM-03	Md	10.5	20.0	30.4	13.1	12.1

The graphical representation of Cr-Th [29] shows that the analyzed samples are mostly distributed around the diorite (Figure 7). In both plots the general trend is the same, giving a distribution that fits well with the continental signature. Comparing them with the values obtained in the Batallones sector located about 3 km to the north, notable differences are observed, taking into account that these are points located at a short distance, with very similar sedimentological and mineralogical characteristics, and in close stratigraphic positions [22].

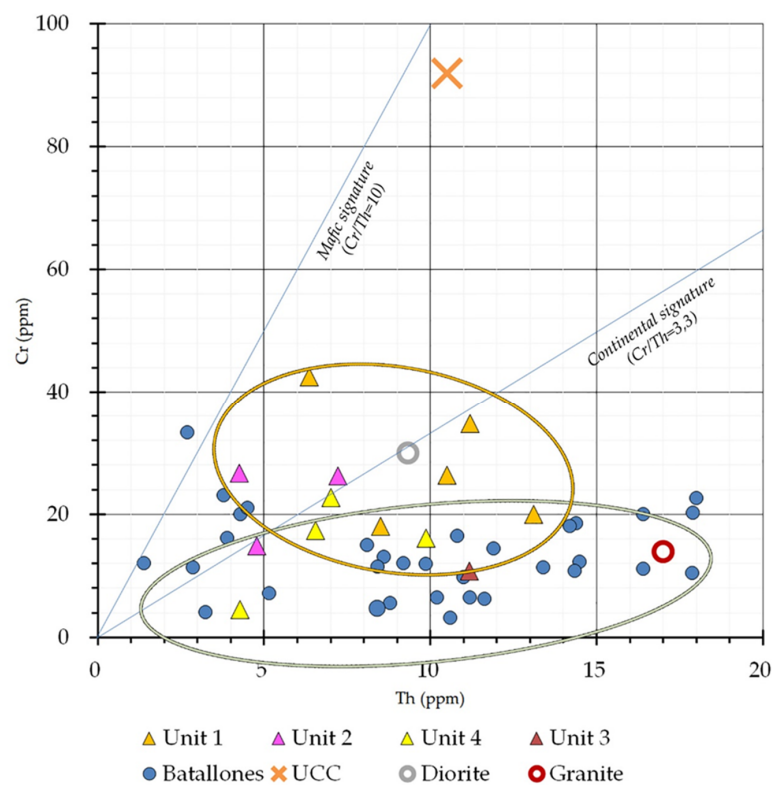


Figure 7. Bivariate plot showing Cr vs. Th contents. Samples from the Batallones sector and compositional references (granite, UCC diorite) are also provided.

A similar result has been obtained using Cr/Th-Sc/Th ratios (Figure 8) and Th/Co-La/Sc (Figure 9) [30] (Figure 8). The studied samples are distributed between granite and diorite compositions. However, the samples analysed in this work are closer to diorites, and again a differential distribution is observed with respect to the samples observed in the nearby Batallones sector [22].

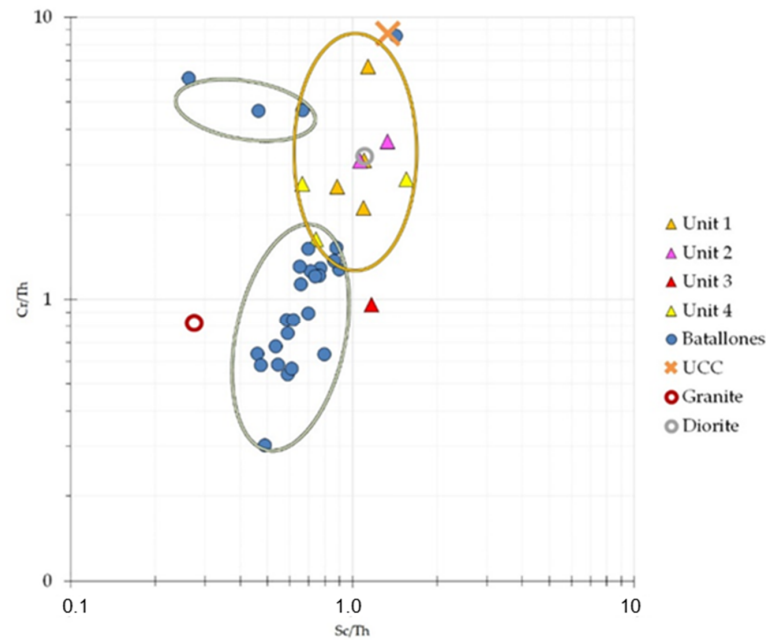


Figure 8. Bivariate plot showing Cr vs. Th contents. Samples from the Batallones sector and compositional references (granite, UCC diorite) are also provided.

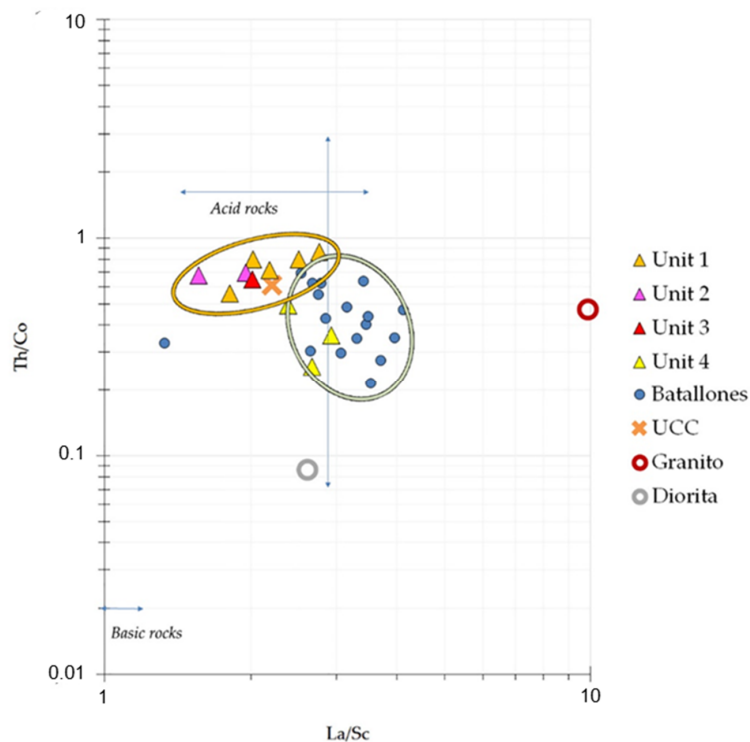


Figure 9. Bivariate plot showing Th/Co vs. La/Sc contents. Samples from the Batallones sector and compositional references (granite, UCC diorite) are also provided.

Based on these graphs, it can be interpreted that the samples analysed show a clear felsic origin, very different from the typical values of basic rocks. Likewise, the differences observed with the samples corresponding to the Batallones sector indicate the existence of more than one source area for the sediments, although in both cases of a felsic character. This would fit well with the participation as parent areas of both the Sistema Central to the north and the Montes de Toledo to the south, which would explain the geochemical differences observed.

4.4. Genetic Considerations of Sepiolite and Associated Authigenic Mg-Clay Minerals

Despite geochemical differences related to the parent area of provenance (Sistema Central, Montes de Toledo, or both) the mineralogical and chemical variations observed in the samples studied fit well with those described for similar materials at Cerro de los Batallones, located a few kilometres to the north [22]. Thus, during the development of unit 1 (and probably unit 3), conditions were such that the influence of surface water was the main factor for the formation of the magnesian clays, with the formation of trioctahedral smectites. The transition to unit 2 involves a drastic change in the environmental conditions (pH, salinity and Mg/Si ratio), with a predominance of lake and groundwater influence, which resulted in a predominance of autigenic processes, in a more restricted saline-alkaline environment with availability of magnesium and silica. At the top of the section, unit 4, shows an abrupt change in the hydrochemical conditions where the role of silica-rich waters is replaced by bicarbonate- and calcium-rich waters. This, however, does not prevent the formation of sepiolite which may be present with palygorskite in this unit.

The origin of these variations would be related to the hydrochemical conditions of formation, a consequence of the interaction between the lithological characteristics of the source area (which makes available Si(OH)_4 , Mg^{2+} and precursor aluminic phases) and the hydrochemistry of the waters involved (surface, ground and lake waters) [31]. The genetic processes involved are shown in Figure 10.

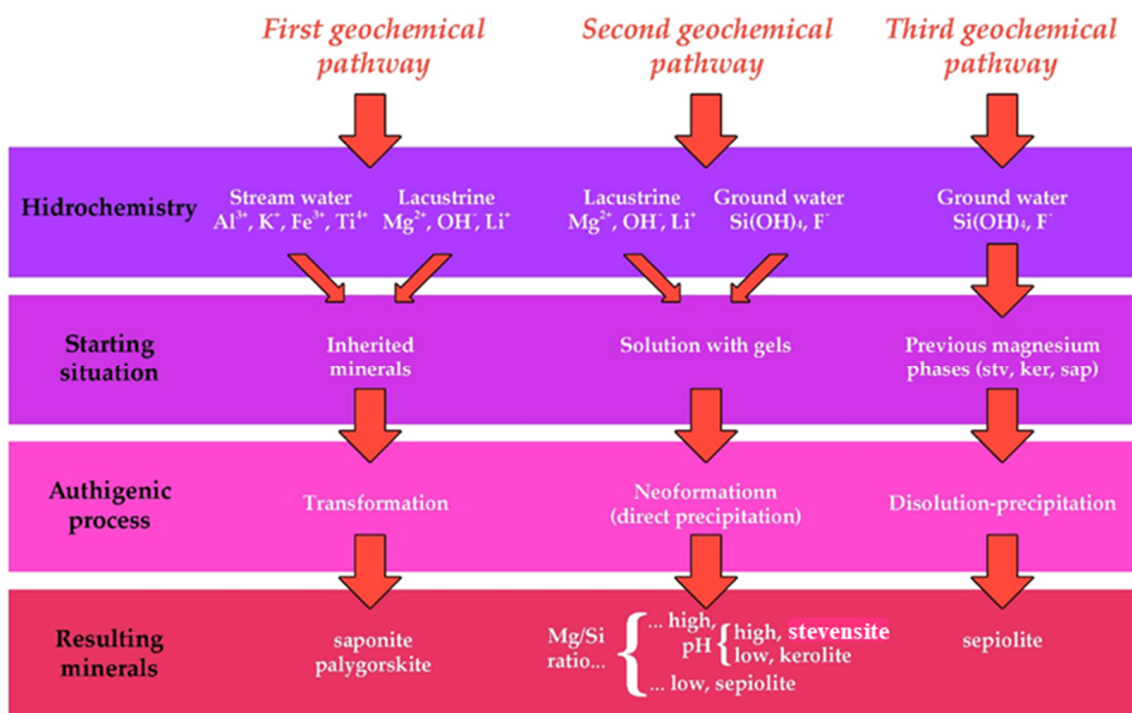


Figure 10. Geochemical processes involved in the formation of magnesian clay minerals.

A first genetic process would be related to the transformation of inherited minerals into magnesian clay minerals containing some aluminium [10]. This process would result in the autigenesis of palygorskite and saponite, as a result of the interaction of saline-alkaline

fluids (such as those present in lake waters) rich in Mg^{2+} with Al-rich inherited minerals. In the materials studied, the formation of trioctahedral smectites from inherited precursors seems to be evident, although this transformation would not be complete. Likewise, the presence of palygorskite in unit 4 is indicative of genesis from aluminic precursors, mainly Al-smectite.

A second genetic process involves the neoformation of new clay minerals by direct precipitation from a solution or gel [10,32]. In this case, the sepiolite in units 2 and 4 would have been formed by this mechanism. In the case of unit 2, mixing between Mg-rich lacustrine fluids and silica-rich subsurface fluids would have led to the formation of mostly sepiolite. In the case of unit 4, variations in the pH of the fluids as a consequence of CO_2 capture when carbonates formed, as well as the concentration of the interstitial solutions, would have favoured the neoformation of the fibrous clay mineral.

The third genetic process would be related to the formation of magnesian clay minerals from magnesian precursors. During diagenesis, changes in the hydrochemistry of surface, lake and groundwater can lead to the formation of sepiolite by transformation (dissolution-precipitation) of other magnesian clays [10]. A drastic change in salinity-pH conditions due to water-mixing and the arrival of silica during the early diagenesis of magnesian smectites favours the formation of intrasedimentary sepiolite [33–36]. This process seems to be evident at the top of unit 1 and the base of unit 2 where there is evidence of sepiolite formation from trioctahedral smectite-rich materials.

The variation in the size of the sepiolite fibres is very small in the processes of transformation of previous magnesian phases, increasing their sizes in the palustrine episodes where they have the possibility of recrystallisation. The crystallinity values based on the FWHM parameter are also significant,

The mineralogical change observed in unit 4 indicates a significant change at the basin level where there is a freshening of the waters that favours the precipitation of carbonates, coinciding with an expansive phase of the lacustrine-palustrine system. In palustrine conditions, the formation of sepiolite shows the capacity of this mineral to form under variable salinity and pH conditions, corroborating the experimental results obtained by [37].

The conditions necessary for the formation of sepiolite are based on the presence of a fluid with a moderate to high basic pH, adequate concentrations of magnesium and silica and the absence of dissolved aluminium [7,10]. These conditions have been reproduced in the laboratory [37], obtaining low crystallinity sepiolite at different pH, salinity and Mg/Si ratios than those required for kerolite or stevensite formation. At low salinity ($NaCl = 0.00$ mol/kg) the precipitation of sepiolite can occur for pH between 8.7 and 9, depending on the concentration of Mg/Si (being able to form at lower pH if the concentration Mg/Si is high). At relatively high salinities ($NaCl = 0.46$ mol/kg) and low Mg/Si concentration, pH controls sepiolite precipitation. These results show that the formation of sepiolite can occur in a wide range of salinities, depending on Mg/Si and pH concentrations, supporting the results obtained using isotopic analysis [38].

The formation of magnesian smectite and palygorskite is controlled by several physico-chemical parameters including pH (alkalinity), PCO_2 and salinity [39]. The role of aqueous CO_2 in the formation of magnesian clay minerals under evaporative conditions is very important because of its strong effect on pH [40]. Palygorskite in particular is commonly formed in lacustrine-palustrine environments [41]. The type of formation of saponite depends on Al-particle availability. The process is particularly favoured where the proportion of sediment to water is high and where the solute content is significant, consistent with the model proposed by Jones [2].

A detailed bibliographical compilation of the formation of the clay minerals described and their relationship with the lacustrine-palustrine environment can be found in [10]

5. Conclusions

1. Mineralogical analysis of lithofacies deposited in a lacustrine margin shows the relationship between palustrine conditions and the authigenic formation of magnesian

clay minerals. Among the mud-flat deposits, two palustrine episodes originating from different hydrochemical conditions with concentrated and dilute water have been identified. The shift from one type of palustrine record to the other indicates an evolution towards freshening conditions in the basin, which is reflected in the lacustrine-palustrine context.

2. In the mud-flat deposits, the presence of trioctahedral phases is interpreted as the formation of magnesian smectite of the saponite type, which would be the result of the transformation of Al-rich inherited minerals. The abundance of magnesium in the environment favoured the development of dolocretes in these deposits.
3. In palustrine deposits with concentrated saline-alkaline water, the formation of sepiolite is favoured, which in a first phase would take advantage of supports with magnesian smectite (possibly stevensite) for its formation, followed by direct precipitation from solutions and/or gels (neof ormation).
4. In palustrine deposits with more dilute water, there are abundant carbonates where the existence of morphologies similar to seepage mounds indicate the active role of groundwater. Under these conditions, sepiolite and palygorskite form in thin beds inserted between the carbonates. The palygorskite would have formed as a result of the transformation of aluminous smectite into the fibrous clay mineral. Sepiolite in the absence of reactive aluminium would have formed by neof ormation.
5. The supply of silica is justified by the existence of a felsic source area of diorite-to-granite type, with geochemical characteristics that suggest the participation of two source areas that supplied the sediments in the studied area. Variations in the hydrochemical characteristics of the water in the lacustrine-palustrine environment were responsible for the authigenic mineral assemblages identified.
6. The results obtained confirm that sepiolite can be formed in a wide range of salinity and pH, confirming the results reported in laboratory synthesis tests. It also corroborates that the formation of magnesian smectite (saponite) or palygorskite by transformation of inherited Al-smectite depends on the hydrochemistry of the water in the sedimentary environment.

Author Contributions: Conceptualization, M.P.; methodology, M.P.; investigation, J.E.H. and M.P.; resources, M.P.; writing—original draft preparation, J.E.H. and M.P.; writing—review and editing, M.P.; visualization, M.P.; supervision, M.P.; project administration, M.P.; funding acquisition, M.P. All authors have read and agreed to the published version of the manuscript.

Funding: The work is part of the scientific activities of research group GPG-418 (UAM).

Data Availability Statement: Not applicable.

Acknowledgments: The authors are grateful to MINER S.A. for the authorization, information, and supply of the studied samples.

Conflicts of Interest: The authors declare no conflict of interest.

References

1. Millot, G. *Geology of Clays*; Springer: Berlin/Heidelberg, Germany, 1970.
2. Jones, B.F. Clay mineral diagenesis in lacustrine sediments. *U.S. Geol. Surv. Bull.* **1986**, *1578*, 291–300.
3. Galán, E.; Pozo, M. Palygorskite and sepiolite deposits in continental environments. Description, genetic patterns and sedimentary settings. In *Developments in Palygorskite–Sepiolite Research. A New Outlook on These Nanomaterials. Developments in Clay Science*; Galán, E., Singer, A., Eds.; Elsevier: Amsterdam, The Netherlands, 2011; pp. 125–173.
4. Lasaga, A. *Kinetic Theory in the Earth Sciences*; Princeton University Press: Princeton, NJ, USA, 1998; pp. 1–811.
5. Zhang, J.; Huang, F.; Lin, Z. Progress of nanocrystalline growth kinetics based on oriented attachment. *Nanoscale* **2010**, *2*, 18–34. [[CrossRef](#)] [[PubMed](#)]
6. Deocampo, D.M.; Cuadros, J.; Wing-dudek, T.; Olives, J.; Amouric, M. Saline lake diagenesis as revealed by coupled mineralogy and geochemistry of multiple ultrafine clay phases: Pliocene Olduvai Gorge, Tanzania. *Am. J. Sci.* **2009**, *309*, 834–868. [[CrossRef](#)]
7. Tosca, N. Geochemical pathways to Mg-silicate formation. In *Magnesian Clays: Characterization, Origin and Applications*; Pozo, M., Galán, E., Eds.; AIPEA Educational Series, Pub. No. 2; Digilabs: Bari, Italy, 2015; pp. 283–330.

8. Guggenheim, S. Introduction to Mg-Rich clay minerals: Structure and composition. In *Magnesian Clays: Characterization, Origin and Applications*; Pozo, M., Galán, E., Eds.; AIPEA Educational Series, Pub. No. 2; Digilabs: Bari, Italy, 2015; pp. 1–62.
9. Pozo, M.; Galán, E. (Eds.) Magnesian clay deposits: Mineralogy and origin. In *Magnesian Clays: Characterization, Origin and Applications*; AIPEA Educational Series, Pub. No. 2; Digilabs: Bari, Italy, 2015; pp. 175–228.
10. Pozo, M.; Calvo, J.P. An Overview of Authigenic Magnesian Clays. *Minerals* **2018**, *8*, 520. [[CrossRef](#)]
11. De Vicente, G.; Cloething, S.; Van Wees, J.D.; Cunha, P.P. Tectonic classification of Cenozoic Iberian foreland basins. *Tectonophysics* **2011**, *502*, 38–61. [[CrossRef](#)]
12. Calvo, J.P.; Alonso-Zarza, A.M.; García del Cura, M.A. Models of Miocene marginal lacustrine sedimentation in response to varied depositional regimes and source areas in the Madrid Basin (central Spain). *Palaeogeogr. Palaeoclimatol. Palaeoecol.* **1989**, *70*, 199–214. [[CrossRef](#)]
13. Calvo, J.P.; Jones, B.F.; Bustillo, M.; Fort, R.; Alonso-Zarza, A.M.; Kendall, C. Sedimentology and geochemistry of carbonates from lacustrine sequences in the Madrid Basin, Central Spain. *Chem. Geol.* **1995**, *123*, 173–191. [[CrossRef](#)]
14. Pozo, M.; Casas, J. Distribucion y caracterizacion de litofacies en el yacimiento de arcillas magnesicas de Esquivias (Neogeno de la Cuenca de Madrid). *Boletín Geológico Y Min.* **1994**, *106*, 265–282.
15. Galán, E.; Castillo, A. Sepiolite–Palygorskite in Spanish Tertiary Basins: Genetical Patterns in Continental Environments. In *Palygorskite–Sepiolite. Occurrences, Genesis and Uses. Developments in Sedimentology*; Singer, A., Galán, E., Eds.; Elsevier: Amsterdam, The Netherlands, 1984; pp. 87–124.
16. Ordóñez, S.; Calvo, J.P.; García del Cura, M.A.; Alonso Zarza, A.M.; Hoyos, M. Sedimentology of sodium sulphate deposits and special clays from the Tertiary Madrid Basin (Spain). In *Lacustrine Facies Analysis. Special Publications International Association of Sedimentologists*; Anadón, P., Cabrera, L., Kelts, K., Eds.; Blackwell Scientific Publications: Oxford, UK, 1991; pp. 39–55.
17. Pozo, M.; Calvo, J.P.; Pozo, E.; Moreno, A. Genetic constraints on crystallinity, thermal behaviour and surface area of sepiolite from the Cerro de los Batallones deposits (Madrid Basin, Spain). *Appl. Clay Sci.* **2014**, *91–92*, 30–45. [[CrossRef](#)]
18. Schultz, L.G. Quantitative interpretation of mineralogical composition from X-ray and chemical data for the Pierre Shale. *Geol. Surv. Prof. Pap.* **1964**, *391*, 31.
19. Van der Marel, H.W. Quantitative analysis of clay minerals and their admixtures. *Contrib. Miner. Pet.* **1966**, *12*, 96–138. [[CrossRef](#)]
20. Chung, F.H. Quantitative Interpretation of X-ray Diffraction Patterns of Mixtures. I. Matrix-Flushing Method for Quantitative Multicomponent Analysis. *J. Appl. Cryst.* **1974**, *7*, 519–525. [[CrossRef](#)]
21. Sánchez del Río, M.; Doménech, A.; Doménech-Carbó, M.T.; Vázquez de Agredos Pascual, M.L.; Suárez, M.; García-Romero, E. The Maya Blue Pigment. In *Developments in Palygorskite–Sepiolite Research. A New Outlook on These Nanomaterials. Developments in Clay Science*; Elsevier: Amsterdam, The Netherlands, 2011; pp. 453–481.
22. Herranz, J.E.; Pozo, M. Authigenic Mg-Clay Minerals Formation in Lake Margin Deposits (the Cerro de los Batallones, Madrid Basin, Spain). *Minerals* **2018**, *8*, 418. [[CrossRef](#)]
23. Pozo, M.; Casas, J.; Medina, J.; Calvo, J.P.; Silva, P.G. Caracterización de depósitos carbonáticos ligados a paleosurgencias en el sector de Batallones-Malcovadeso (Neógeno de la cuenca de Madrid). *Estud. Geológicos* **2006**, *62*, 73–88. [[CrossRef](#)]
24. González, J.M.; Bauluz, B.; Fernández-Nieto, C.; Yuste, A. Factors controlling the trace-element distribution in fine-grained rocks: The Albian kaolinite-rich deposits of the Oliete Basin (NE Spain). *Chem. Geol.* **2005**, *214*, 1–19.
25. McLennan, S.M.; Nance, W.B.; Taylor, S.R. Rare earth element-thorium correlations in sedimentary rocks, and the composition of the continental crust. *Geochim. Cosmochim. Acta* **1980**, *44*, 1833–1839. [[CrossRef](#)]
26. Rollinson, H.R. *Using Geochemical Data: Evaluation, Presentation, Interpretation*; Pearson Education Limited: London, UK, 1993.
27. McLennan, S.M.; Hemming, S.; McDaniell, D.K.; Hanson, G.N. Geochemical approaches to sedimentation, provenance, and tectonics. In *Processes Controlling the Composition of Clastic Sediments*; Johnsson, M.J., Basu, A., Eds.; Geological Society of America: Boulder, CO, USA, 1993.
28. Condie, K.C. Chemical composition and evolution of the upper continental crust: Contrasting results from surface samples and shales. *Chem. Geol.* **1993**, *104*, 1–37. [[CrossRef](#)]
29. Grizelj, A.; Tibljas, D.; Kovacic, M. Mineralogy and geochemistry of Upper Miocene pelitic sediments of the Zagorje Basin (Croatia): Implication for evolution of the Pannonian Basin. *Geol. Carpathica* **2007**, *58*, 263–276.
30. Condie, K.C.; Wronkiewicz, D.J. The Cr/Th ratio in Precambrian pelites from the Kaapvaal Craton as an index of craton evolution. *Earth Planet. Sci. Lett.* **1990**, *97*, 256–267. [[CrossRef](#)]
31. Pozo, M. Origin and evolution of magnesium clays in lacustrine environments: Sedimentology and geochemical pathways. In *Proceedings of the First Latin-American Clay Conference, Invited Lectures, Funchal, Madeira, Portugal, 17–22 September 2000*; Volume 1, pp. 117–133, ISBN: 972 98383 4 8.
32. Calvo, J.P.; Pozo, M. Geology of magnesian clays in sedimentary and non-sedimentary environments. In *Magnesian Clays: Characterization, Origin and Applications*; Pozo, M., Galán, E., Eds.; AIPEA Educational Series, Pub. No. 2; Digilabs: Bari, Italy, 2015; pp. 123–174.
33. Eberl, D.D.; Jones, B.F.; Khoury, H.N. Mixed-layer kerolite/stevensite from the Amargosa Desert, Nevada. *Clays Clay Miner.* **1982**, *30*, 321–326. [[CrossRef](#)]
34. Khoury, H.N.; Eberl, D.D.; Jones, B.F. Origin of magnesium clays from the Amargosa Desert, Nevada. *Clays Clay Miner.* **1982**, *30*, 327–336. [[CrossRef](#)]

35. Pozo, M.; Medina, J.A.; Leguey, S. Mineralogénesis de palygorskita en la zona central de la Cuenca de Madrid. *Boletín De La Soc. Española Mineral.* **1985**, *8*, 271–283.
36. Pozo, M.; Casas, J.C. Origin of kerolite and associated Mg clays in palustrine– lacustrine environments. The Esquivias deposit (Neogene Madrid Basin, Spain). *Clay Miner.* **1999**, *34*, 395–418. [[CrossRef](#)]
37. Tosca, N.J.; Masterson, A.L. Chemical controls on incipient Mg-silicate crystallization at 25 °C: Implications for early and late diagenesis. *Clay Miner.* **2014**, *49*, 165–194. [[CrossRef](#)]
38. Clauer, N.; Fallick, A.E.; Galán, E.; Pozo, P.; Taylor, C. Varied crystallization conditions for neogene sepiolite and associated Mg-Clays from Madrid Basin (Spain) traced by oxygen and hydrogen isotope geochemistry. *Geochim. Cosmochim. Acta* **2012**, *94*, 181–198. [[CrossRef](#)]
39. Jones, B.F.; Galán, E. Sepiolite and palygorskite. In *Hydrous Phyllosilicates*; Bailey, S.W., Ed.; Reviews in Mineralogy; Mineralogy Society of America: Chantilly, VA, USA, 1988; pp. 631–674.
40. Deocampo, D.M. Evaporative evolution of surface waters and the role of aqueous CO₂ in magnesium silicate precipitation: Lake Eyasi and Ngorongoro Crater, northern Tanzania. *S. Afr. J. Geol.* **2005**, *108*, 493–504. [[CrossRef](#)]
41. Webster, C.E.; Jones, B.F. Paleoenvironmental implications of lacustrine clay minerals from the Double Lakes formation, southern High Plains, Texas. In *Sedimentology and Geochemistry of Modern and Ancient Saline Lakes*; Renaut, R.W., Last, W.L., Eds.; SPEM (Society for Sedimentary Geology): Tulsa, OK, USA, 1994; pp. 159–172.